Exploring the shear strain contribution to the uniaxial magnetic anisotropy of (Ga,Mn)As

M Kraimia, L. Largeau, K. Boujdaria, B. Croset, C. Mocuta, A. Lemaitre, C. Gourdon, L. Thevenard

Exploring the shear strain contribution to the uniaxial magnetic anisotropy of (Ga,Mn)As

M. Kraimia,[1,2] L. Largeau,[3] K. Boujdaria,[2] B. Croset,[1] C. Mocuta,[4] A. Lemaître,[3] C. Gourdon,[1] and L. Thevenard[1,*]

[1] *Sorbonne Université, CNRS, Institut des Nanosciences de Paris, 4 place Jussieu,75252 Paris France*
[2] *Université de Carthage, Faculté des Sciences de Bizerte, LR01ES15 Laboratoire de Physique des Matériaux: Structure et Propriétés, 7021 Zarzouna, Bizerte,Tunisia*
[3] *Centre de Nanosciences et de Nanotechnologies, CNRS, Univ. Paris-Sud, Université Paris-Saclay, 91120 Palaiseau, France*
[4] *Synchrotron SOLEIL, L'Orme des Merisiers Saint-Aubin, F-91192 GIF-sur-YVETTE CEDEX*

We present an experimental and **k.p** theoretical study on the origin of the strong in-plane uniaxial magnetic anisotropy in (Ga,Mn)As layers, unexpected from the cubic crystalline structure. The symmetry lowering can be accounted for by structural or effective shear strains. We find theoretically out-of-plane and in-plane magnetic anisotropy constants linear with the shear strain. Searching for a real shear strain arising from lattice relaxation we perform two types of measurements: anomalous X-ray diffraction and strain-induced optical birefringence, at room temperature. Working on a strongly anisotropic (Ga,Mn)As layer, the estimated $\epsilon_{xy} = 10^{-4}$ was not found although it lied an order of magnitude above the detection threshold. This ensemble of results indicates as unlikely a relaxation-driven uniaxial anisotropy. As previously suggested theoretically, the magnetic symmetry-lowering could instead originate from the anisotropic incorporation of Mn atoms during the growth. This would yield a perfectly in-plane matched lattice, with an anisotropy that could nevertheless be modelled as an *effective* shear strain, and modified by an external shear stress, in agreement with the existing experimental literature.

INTRODUCTION

Uniaxial anisotropy in ferromagnetic layers, tracks, and nanostructures is a key factor for technological applications such as the straightforward encoding of "0" and "1" bits for memory and storage devices. Materials with out-of-plane (OP) uniaxial anisotropy have for instance been used to increase storage density in perpendicular magnetic recording [1]. In various schemes for non-inductive magnetization manipulation and switching, in-plane (IP) uniaxial anisotropy offers an alternate and versatile option for fixing the magnetization easy axis, avoiding to rely only on shape anisotropy [2–4].

Whereas OP uniaxial anisotropy is fairly well understood [5, 6], much less is known about the origin of IP uniaxial anisotropy. It can arise for instance from an interfacial effect [7], anisotropic grain domains [8], or anisotropic relaxation of the epitaxial strain [8, 9]. It can be obtained by molecular beam epitaxy such as in Fe/GaAs [10–12] and the semiconductor (Ga,Mn)As [6, 13–19], or with better control by various other growth techniques [20, 21].

In layers of (Ga,Mn)$As_{1-y}P_y$ the microscopic origin of an IP uniaxial anisotropy constant $K_{2\|}$ has been the subject of many experimental and theoretical investigations [6, 13, 19, 22–25]. From symmetry considerations and band theory calculation in the **k.p** approximation, it was soon recognized that an ϵ_{xy} strain, which may result from different strains along the [110] and [-110] directions, could explain this magnetic anisotropy and its dependence with the carrier density and temperature [6, 18]. The value of $\epsilon_{xy} \approx 1-5\ 10^{-4}$ obtained from these calculations was reasonably small, lower than the epitaxial strain by one order of magnitude. Whether the ϵ_{xy} strain is a real strain or the parameter of a perturbation Hamiltonian lowering the symmetry of the zinc blende crystal has been the subject of a long-standing debate, not yet settled.

Experimental results have repeatedly evidenced the modification of the IP uniaxial anisotropy via strain, e.g using a piezoelectric transducer to apply stress [22], or deep etching of narrow bars to relax the epitaxial strain anisotropically [14]. It has also been shown that thin (Ga,Mn)As bars oriented along the [110], [100], and [-110] directions relax differently, leading to varying magnetic anisotropies [16]. A shear strain-dependence of the anisotropy also seems necessary to account for surface acoustic wave (SAW) driven magnetization excitation and switching in IP magnetized (Ga,Mn)As through the magnetoelastic interaction [26, 27]. The microscopic origin of this IP symmetry breaking would for instance be the [110]/[-110] anisotropic incorporation of Mn atoms due to stacking faults [25], or Mn dimer formation [13, 23] due to GaAs surface reconstruction [12, 28, 29]. This could either lead to a genuine IP strain relaxation, potentially detectable experimentally, or to a built-in shear *stress* which would be virtually undetectable once the layer resting in perfect epitaxy onto its substrate.

Another approach is to consider that, from a macroscopic point of view, any depth dependence of the magnetic properties could lower the crystal symmetry from D_{2d} to C_{2v} hence making the [110] and [-110] directions non-equivalent. However there is no clear systematic experimental evidence of such depth dependence [9, 15, 30–

32]. The dissymmetry of the two interfaces has also been invoked, since the existence of a spin-orbit field arising from the Rashba inversion asymmetry term [33, 34] or the Dzyaloshinskii-Moriya interaction [35] reveals the breaking of the z-symmetry. Yet a pure interfacial origin of the IP uniaxial magnetic anisotropy was ruled out by a thickness-dependence study [15].

In this report, we investigate theoretically and experimentally the shear-strain origin of IP anisotropy in (Ga,Mn)As layers. While the few reports of X-ray diffraction on such samples have not shown any difference of the lattice parameter along [110] and [-110] [15, 25], we renew the attempt to reveal a static ϵ_{xy} shear strain by working on thinner and more magnetically anisotropic layers, and combining different experimental techniques. Using the band structure obtained from the **k.p**, exchange and strain Hamiltonians, we first determine the parameters (exchange, carrier density, and static shear strain) consistent with the measured magnetic anisotropy constants. Two very different experiments are then shown, aiming to reveal the presence of the estimated 10^{-4} shear strain: direct observation of the in-plane lattice by X-ray diffraction, and photoelasticity-induced optical birefringence. This ensemble of results point to an upper boundary of a few 10^{-5} for any genuine shear strain. This rules out anisotropic IP strain relaxation as the main origin of the uniaxial anisotropy in (Ga,Mn)As and favors alternative scenari instead.

EXPERIMENTAL UNIAXIAL ANISOTROPIES

Correlation between OP and IP anisotropy constants

Phenomenologically, the magnetic free energy in the absence of applied magnetic field is defined as [36]:

$$E_m = -K_{2\perp}\cos^2\theta - K_{2\parallel}\sin^2\theta\sin^2\left(\phi-\frac{\pi}{4}\right) - \frac{K_{4\parallel}}{8}\sin^4\theta(3+\cos(4\phi)) - \frac{K_{4\perp}}{2}\cos^4\theta - \frac{\mu_0}{2}M_S^2\sin^2\theta \quad (1)$$

where $K_{2\perp}$ and $K_{2\parallel}$ are the uniaxial OP and IP anisotropy constants, respectively, and $K_{4\parallel}$ and $K_{4\perp}$ are the cubic anisotropy constants. The last term represents the shape anisotropy and depends on the saturation magnetization M_s. Angles ϕ and θ are counted with respect to [100] IP and [001] OP axes, respectively.

Putting together experimental OP and IP anisotropy constants of numerous (Ga,Mn)As and (Ga,Mn)(As,P) samples, one notices that $K_{2\parallel}$ is roughly proportional to $K_{2\perp}$ for compressively strained samples (Fig. 1). This seems unrelated to the effective concentration of Mn atoms, the presence of phosphorus or the layer thickness. The slope of $K_{2\parallel}$ versus $K_{2\perp}$ itself seems linked to the degree of optimization of the annealing step, as clearly comes out when comparing the data of Ref. [32] with the others [37]. For tensile layers however, OP and IP anisotropies seem uncorrelated, but [1-10] remains the easier IP axis, like for the compressed samples. Since the OP anisotropy varies linearly with the lattice mismatch (lm) between the layer and the substrate, we postulate that large shear strain might appear in the case of large positive lm owing to anisotropic strain relaxation. Therefore we investigate the origin of the IP uniaxial anisotropy in two samples of similar Mn concentration, one with strong IP uniaxial anisotropy (sample A), and the other with biaxial anisotropy (sample B).

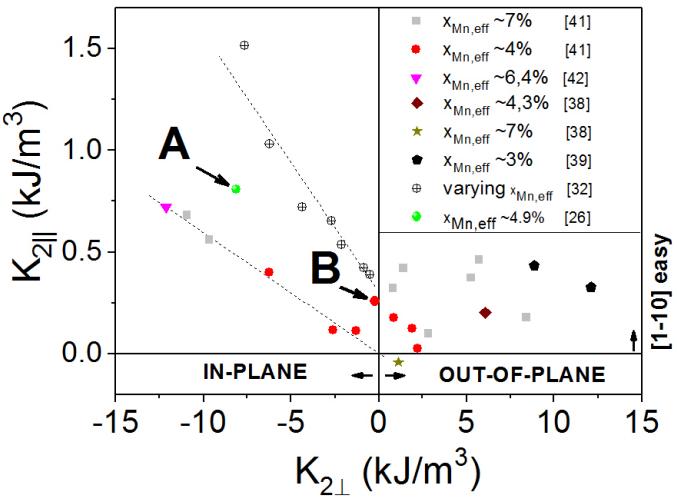

FIG. 1. Experimental uniaxial IP anisotropy constants $K_{2\parallel}$ versus uniaxial OP anisotropy constant $K_{2\perp}$ for several sets of (Ga,Mn)As [26, 32, 38, 39] and (Ga,Mn)(As,P) [38–42] epitaxial layers at low temperature. Dashed lines are guides for the eyes. All layers are 50 nm thick except in Refs. [42] (200 nm) and [32] (25 nm). Samples from Ref. [32] were highly optimized (choice of growth temperature, and long anneal times in particular). Samples from Refs. [38–41] underwent a standard 1 h/250 °C anneal, while sample A underwent a somewhat intermediate anneal of 16 h/200 °C [26].

Samples

In the following we detail the characteristics of the two samples, both grown by molecular beam epitaxy on a (001) GaAs substrate topped with a high growth temperature (600°C) ≈ 500 nm GaAs buffer. Sample A consists of a (Ga,Mn)As layer of thickness 45 nm with an effective Mn concentration $x_{\rm eff}$=5 %. It was annealed for 16 h at 200°C. The Curie temperature is 120 K and M_s is 51.3 kA m^{-1} at T=4 K. The strained lattice mismatch after the anneal is lm=3860 ppm, resulting in a biaxial epitaxial compressive in-plane strain

$\epsilon_{xx} = \epsilon_{yy} = -2\ 10^{-3}$. The magnetic anisotropy constants obtained by ferromagnetic resonance (FMR) at T=4 K are $K_{2\perp}$=-8.5 kJ m^{-3}, $K_{2\parallel}$=1 kJ m^{-3} and $K_{4\parallel}$=0.41 kJ m^{-3}. The easy magnetic axis is IP along the [-110] direction. In this sample the magnetoelastic coupling has been well established from SAW-induced magneto-acoustic resonance and magnetization switching [26, 27]. A model using the B_2 magnetoelastic constant (see further in the article) obtained from the experimental value of $K_{2\parallel}$ and the value of ϵ_{xy} estimated from the **k.p** calculation quantitatively accounted for the amplitude of SAW-induced magnetization precession, suggesting the magnetoelastic origin of $K_{2\parallel}$.

Sample B is a (Ga,Mn)$As_{0.95}P_{0.04}$ layer of thickness 50 nm with x_{eff}=4 %. It was annealed for 1 h at 250°C. The Curie temperature is 85 K. At T=4 K the saturation magnetization is 40.7 kA m^{-1}, the anisotropy constants are $K_{2\perp}$=-0.22 kJ m^{-3}, $K_{2\parallel}$=0.26 kJ m^{-3}, and $K_{4\parallel}$=1.57 kJ m^{-3}. The strained lattice mismatch is lm=-1200 ppm ($\epsilon_{xx} = -6\ 10^{-4}$). The OP anisotropy resulting from the small tensile strain is weaker than the shape anisotropy resulting in IP magnetization with biaxial magnetic anisotropy and easy axes close to the <100> IP directions since $K_{2\parallel} \ll K_{4\parallel}$. In this sample, easy triggering of spin wave excitation by optical pulses was demonstrated [43].

In the following section we will use the lattice mismatch obtained at room temperature in order to model the band structure and magnetic uniaxial anisotropies in the low temperature limit. This procedure, used by many authors without questioning, is actually justified by the identical temperature dependence of the perpendicular lattice parameters of (Ga,Mn)As and GaAs [44].

MODELLING UNIAXIAL ANISOTROPIES

Methodology

The magnetic anisotropy properties are studied in the framework of the effective mass approximation by using the following total Hamiltonian $\mathcal{H} = \mathcal{H}_{\mathbf{kp}} + \mathcal{H}_{exc} + \mathcal{H}_S$. $\mathcal{H}_{\mathbf{kp}}$ is the six-band Kohn-Luttinger Hamiltonian [45], which was shown to be sufficient for (Ga,Mn)As for a Fermi energy up to $\simeq$ 300 meV [46]. We employ GaAs values for the Luttinger parameters [47]. $\mathcal{H}_{exc}$ describes the effective exchange interaction between the delocalized hole spin s and the localized Mn spin S ($S = \frac{5}{2}$) arising from p–d hybridization [48, 49]. In the mean field approximation in which the virtual crystal approximation is made [49], one can write the exchange interaction as ($-x_{\text{eff}} N_0 \beta_{pd} < S > s$). N_0 is the cation sites concentration, β_{pd} the p–d exchange integral. x_{eff} is the effective Mn concentration which is deduced from the low-temperature saturation magnetization M_s by $x_{\text{eff}} = \frac{M_s}{N_0 S\, g\, \mu_B}$, where g is the Landé factor and μ_B the Bohr magneton. The strain effects are modeled by the Bir-Pikus Hamiltonian $\mathcal{H}_S$ [50]. Formally, this strain Hamiltonian has the same structure as the Kohn-Luttinger Hamiltonian in which $k_\alpha k_\beta$ is replaced by $\epsilon_{\alpha\beta}$, and the Luttinger parameters are replaced by the deformation potentials, namely a_v, b_v and d_v (for more details, see for example Ref. [6]). In the basis given in [51] [52] it takes the following expression:

$$\mathcal{H}_S = \begin{pmatrix} (A_{1s}-A_{2s}) & B_s & C_s & 0 & \frac{1}{\sqrt{2}}B_s & \sqrt{2}C_s \\ cc & (A_{1s}+A_{2s}) & 0 & C_s & \sqrt{2}A_{2s} & -\sqrt{\frac{3}{2}}B_s \\ cc & 0 & (A_{1s}+A_{2s}) & -B_s & -\sqrt{\frac{3}{2}}B_s^* & -\sqrt{2}A_{2s} \\ 0 & cc & cc & (A_{1s}-A_{2s}) & -\sqrt{2}C_s^* & \frac{1}{\sqrt{2}}B_s^* \\ cc & cc & cc & cc & A_{1s} & 0 \\ cc & cc & cc & cc & 0 & A_{1s} \end{pmatrix} \quad (2)$$

where cc denotes the complex conjugate. One writes the non-zero matrix elements of $\mathcal{H}_S$ as:

$$A_{1s} = a_v(\epsilon_{xx} + \epsilon_{yy} + \epsilon_{zz}) \quad (3)$$

$$A_{2s} = \frac{b_v}{2}(\epsilon_{xx} + \epsilon_{yy} - 2\epsilon_{zz}) \quad (4)$$

$$B_s = d_v(\epsilon_{zx} - i\epsilon_{zy}) \quad (5)$$

$$C_s = \frac{\sqrt{3}}{2} b_v(\epsilon_{xx} - \epsilon_{yy}) - i d_v \epsilon_{xy} \quad (6)$$

Adopting the notation of Glunk *et al.* [53] for the relaxed lattice parameter and strain, one can write $\epsilon_{zz} = \frac{a_\perp - a_{rel}}{a_{rel}}$. a_{rel} is the relaxed lattice parameter of a biaxially strained layer on a [001]-oriented substrate obtained as:

$$a_{rel} = \frac{2C_{12}}{C_{11}+2C_{12}} a_\parallel + \frac{C_{11}}{C_{11}+2C_{12}} a_\perp \ , \quad (7)$$

where $a_\parallel$ and $a_\perp$ are the lateral and vertical lattice parameters of the layer. In our theoretical approach and due to: (i) the $T_d \rightarrow D_{2d}$ symmetry reduction, we consider the biaxial strain components, namely $(\epsilon_{xx}, \epsilon_{yy}, \epsilon_{zz})$ with $\epsilon_{xx} = \epsilon_{yy}$ and $\epsilon_{xx} = -\frac{C_{11}}{2C_{12}}\epsilon_{zz}$, where C_{11} and C_{12} are the elastic constants [54], (ii) the $D_{2d} \rightarrow C_{2v}$ symmetry reduction, the only shear strain component we consider is the ϵ_{xy} that describes the in-plane deformation of the (Ga,Mn)As lattice.

In the following, we restrict our calculations to zero temperature and zero magnetic field. According to the microscopic model [6, 49, 53, 55], we can calculate the carrier contribution to the magnetic free energy. The effective anisotropy field $\mathbf{B}_{\text{eff}}$ acting on the magnetization is equal to -$\nabla_M E_c(\mathbf{M})$, where E_c is the carrier energy density, therefore $E_m = E_c$. Using Eq. B2 of Ref. [49], we evaluate E_c by integrating the Fermi energy with respect to the hole concentration for different magnetization orientations. Note that the main contribution of E_c to the magnetic anisotropy comes from the spin-orbit coupling in the valence band. Once E_c is calculated numerically

as a function of the orientation of the magnetization with respect to the crystalline orientations (θ, ϕ), we compare it with the phenomenological E_m (Eq. 1), excluding shape anisotropy, and deduce the magnetic anisotropy constants.

Uniaxial anisotropy constants without and with shear strain

In Fig. 2(a), $K_{2\perp}$ is plotted as a function of the hole concentration, p, for various exchange splittings of the valence subbands, $B_g = \frac{A_F \beta_{pd} M_s}{6 g \mu_B}$ (A_F is the Fermi-liquid parameter), namely B_g = -20, -30, and -40 meV. Setting aside the shape anisotropy, the sign change of $K_{2\perp}$ is a signature of the change of the magnetic configuration from (001) easy-plane ($K_{2\perp} < 0$) to [001] easy axis ($K_{2\perp} > 0$). The dashed line represents the experimental value of $K_{2\perp}$ for sample A, i.e. $K_{2\perp} = -8.5$ kJ m^{-3}, which is in good agreement with microscopic model prediction, -8.81 kJ m^{-3} when B_g=-40 meV and p=3.5 10^{20} cm^{-3}. Adopting B_g=-40 meV, one estimates $M_s \simeq 68$ kA m^{-1} while the experimental value of the saturation magnetization for sample A is $M_s \simeq 51.3$ kA m^{-1}. This discrepancy might originate from the experimental difficulty in determining M_s giving some error bar. Moreover, the adopted values of β_{pd} and A_F can also explain such discrepancy. Once we have validated the (B_g, p) values, we focus on the shear strain effect on the uniaxial anisotropy constants. This is summarized in Fig. 2(b) which shows $K_{2\perp}$ (black line) and $K_{2\parallel}$ (red line) as a function of ϵ_{xy} strain. The linear dependence of $K_{2\perp}$ and $K_{2\parallel}$ is clearly seen. Such behavior was expected because $K_{2\parallel}$ is roughly proportional to $K_{2\perp}$ as seen in Fig. 1. Considering alternatively the perturbation of the band structure brought by anisotropically distributed Mn dimers, Birowska [23] predicts instead that $K_{2\perp}$ is almost unchanged for a wide range of ϵ_{xy} while observing a linear behavior for $K_{2\parallel}$, contradicting the experimental trend observed in the compressive regime (Fig. 1). As shown in Fig. 2(b), and for $\epsilon_{xy} = 10^{-4}$, one gets $K_{2\perp} = -8.2$ kJ m^{-3} and $K_{2\parallel} = 0.96$ kJ m^{-3} which are in good agreement with the FMR data of sample A, namely $K_{2\perp} = -8.5$ kJ m^{-3} and $K_{2\parallel} = 1$ kJ m^{-3}. The inset of Fig. 2(b) which shows $K_{2\parallel}$ as a function of p confirms the same trend concerning this agreement between our theoretical predictions and the FMR data. The present ϵ_{xy} value is in line with previous estimations following a similar approach, which range from 10^{-4} to 5 10^{-4} [6, 18].

Magnetoelasticity and anisotropy constants

Having evaluated numerically the shear strain needed to yield the experimental $K_{2\perp}$ and $K_{2\parallel}$, we now link the

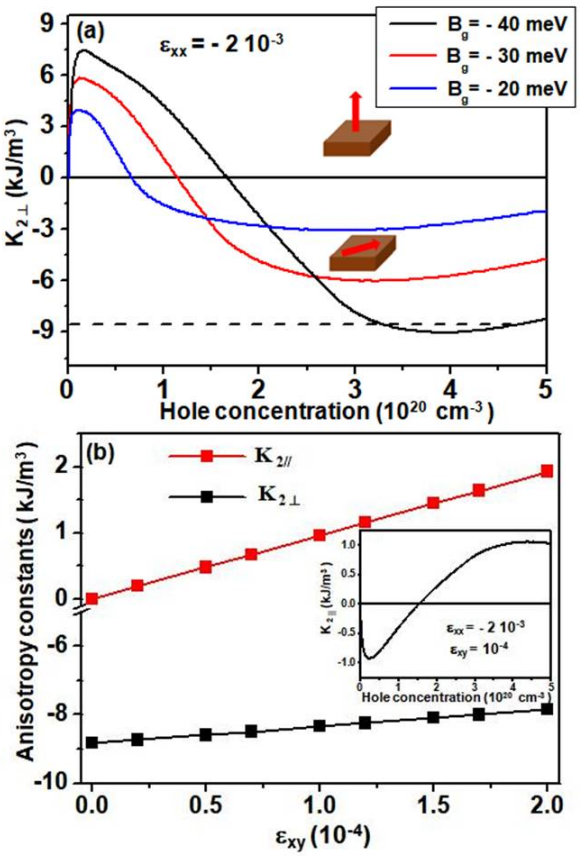

FIG. 2. (a) Perpendicular anisotropy constant $K_{2\perp}$ as a function of the carrier density for different values of the exchange parameter B_g. The dashed line corresponds to the experimental value. (b) Perpendicular uniaxial anisotropy constant $K_{2\perp}$, and in-plane uniaxial anisotropy constant $K_{2\parallel}$ as a function of the shear strain for a carrier density $p = 3.5\ 10^{20}$ cm^{-3}, with $B_g = -40$ meV and $\epsilon_{xx} = -2\ 10^{-3}$. The inset shows $K_{2\parallel}$ as function of the hole concentration with $\epsilon_{xx} = -2\ 10^{-3}$ and ϵ_{xy} =10^{-4}.

phenomenological constants of magnetic anisotropy with the magnetoelastic constants (B_1, B_2). For this purpose, we consider the phenomenological description of the magnetoelastic energy, E_{me}, which describes the interaction between the magnetization and the mechanical strain of the lattice. We start from the general expression of E_{me} in the cubic symmetry case keeping only terms up to the second order in the magnetization components [56]:

$$E_{me} = B_1 \epsilon_{ii} (m_i^2 - \frac{1}{3}) + 2 B_2 \epsilon_{ij} m_i m_j \qquad (8)$$

Without applied magnetic field, the E_{me} energy coincides with the uniaxial components of the magnetic free energy, E_m, explicitly given by Eq(1). Identifying Eq (8) with Eq(1), one can deduce

$$K_{2\parallel} = 2 B_2 \epsilon_{xy} = -6 C_{44} \lambda_{111} \epsilon_{xy} \qquad (9)$$

$$K_{2\perp} = -\frac{2C_{12}+C_{11}}{2C_{12}}B_1\epsilon_{zz} + B_2\epsilon_{xy}$$

$$= \frac{3}{2}\frac{(2C_{12}+C_{11})(C_{11}-C_{12})}{2C_{12}}\lambda_{100}\epsilon_{zz} - 3C_{44}\lambda_{111}\epsilon_{xy} \quad (10)$$

where λ_{100} and λ_{111} are the saturation magnetostriction constants when the magnetization is aligned along the [100] and [111] directions, respectively. Using Eqs (9, 10), we get $\lambda_{100} \simeq -27$ ppm and $\lambda_{111} \simeq -26$ ppm, comparable to values for ferromagnetic magnetostrictive metals such as Ni ($\lambda_{100} \simeq -46$ ppm, $\lambda_{111} \simeq -24$ ppm) [57] and Fe ($\lambda_{100} \simeq 20$ ppm, $\lambda_{111} \simeq -21$ ppm) [57]. These values are about 3 times larger than the ones determined experimentally (8-11 ppm), however on an unannealed sample with low Curie temperature (57 K)[58]. We can also deduce $\lambda_{100} \simeq \lambda_{111}$ indicating a quasi-isotropic magnetostriction for the (Ga, Mn)As compound.

SEARCHING FOR A REAL SHEAR STRAIN

Having estimated the shear strain required to yield the observed anisotropy, we then search for experimental evidence of it using either X-ray diffraction, or the photoelastic effect.

X-ray diffraction

Two strategies requiring different configurations were adopted but conveying both the idea that the IP (Ga,Mn)As lattice has slightly relaxed and become rectangular in the <110> base (Figs. 3(a), 4(a)). In (C1) configuration (Fig. 3(a)), we look for [110] and [1-10] vectors of different lengths (as done in Refs. [15, 25]). For this we perform incident angle (ω-)scan along three 90°-apart IP azimuths. The mapped regions were chosen to cover, in the same dataset, X-ray diffraction signal originating both from the GaAs substrate and the (Ga,Mn)As layer. The shift along Q_x (ΔQ_i) between the substrate and layer peak positions is extracted from the $Q_x - Q_z$ map reconstruction for each azimuth i. From the estimated shear strain for sample A, a maximum of $\frac{\Delta Q_i}{Q_{GaAs}}$-$\frac{\Delta Q_{i+1}}{Q_{GaAs}} \approx 2.10^{-4}$ can be expected for two successive [hh] IP azimuths, and none for diametrically opposed azimuths (i and $i+2$), as shown in the schematics of Fig. 3(a). A similar procedure is then performed along <100> IP directions, for which we expect identical lattice spacing.

In (C2) configuration (Fig. 4(a)), we look for angles between <100> IP directions differing from 90° for the (Ga,Mn)As layer, or equivalently that <100> IP (Ga,Mn)As axes do not coincide with GaAs ones. To do so, azimutal (ϕ) scans are performed around three 90°-spaced IP azimuths i, and compared to [110]/[1-10] scans for which no difference of peak position is expected. Using again ϵ_{xy}=10^{-4}, a maximum spacing of $\Delta\phi$=$\phi_{GaAs,i}$-$\phi_{(Ga,Mn)As,i}$=(-1)^{i}12 mdeg can be anticipated for *h0l* peaks : a signature of shear strain is indeed that the angle between [100]/[010] vectors of (Ga,Mn)As should alternatively be smaller (<90°) or larger (>90°) than for GaAs (see schematics of Fig. 4(a)). For *hhl* peaks, we expect from this scenario $\Delta\phi$= 0 for all azimuths.

Experiments were performed at room temperature on the DiffAbs beamline of the SOLEIL synchrotron. High resolution reciprocal space maps around the various diffraction peaks were performed. By using a hybrid pixel area detector (XPAD) covering an angular range of several degrees, these measurements are typically realized by scanning one of the sample angles / orientations around the value satisfying the Bragg law. Data is acquired during the continuous movement (rotation) of the motor (which is optically encoded) for achieving angular resolution better than 0.1 mdeg. Corresponding volumes in the reciprocal space (Q_x, Q_y, Q_z coordinates) were reconstructed and X-ray diffraction peak position was extracted from 2D planar cuts. Indices *h,k,l* were chosen low enough to have both peaks appearing on the 2D XPAD detector and $l \neq 0$, but large enough to clearly separate GaAs and (Ga,Mn)As peaks for (C1). Although X-ray diffraction using a well collimated X-ray beam (e.g. like the one at a synchrotron facility) is expected to detect such quantities, we should point out here the particular difficulty related to the presence of the very sharp and intense GaAs substrate diffraction peaks located extremely close to the (Ga,Mn)As epitaxial layer peaks. With indices verifying $h+k+l$=$4n+2$ for the (*hhl*) peak, the energy was moreover tuned for anomalous diffraction in order to minimize the GaAs signal [59]. The final configuration was to study (206) and (226) peaks at E=12.35 keV. The X-ray beam spot size was around 150μm. Although anomalous diffraction conditions were fulfilled for (226) planes, the Bragg peak intensity remained over 100 times larger than that of the 45 nm thick magnetic layer, because of the much deeper penetration depth of X-Rays (about 2 μm).

Typical maps and cuts realized in (C1) configuration are shown in Fig. 3(b,c). A systematic difference of IP peak position was observed between the substrate and the sample A layer, corresponding to $\frac{\Delta Q_i}{Q_{GaAs}}$-$\frac{\Delta Q_{i+1}}{Q_{GaAs}} \approx$-2±0.5.$10^{-4}$ for (226) peaks and 1.2±0.5.10^{-4} for (206) peaks. Fairly large deviations were observed between repeated measurements however and no significant difference observed between 2 consecutive or opposite peaks, contrary to what is expected from shear strain. As a result, we could at best conclude on a very marginal isotropic IP relaxation of the layer, but not on any nonequivalent lattice spacing along [110]/[1-10] directions as opposed to [100]/[010] ones. Using this data, we also

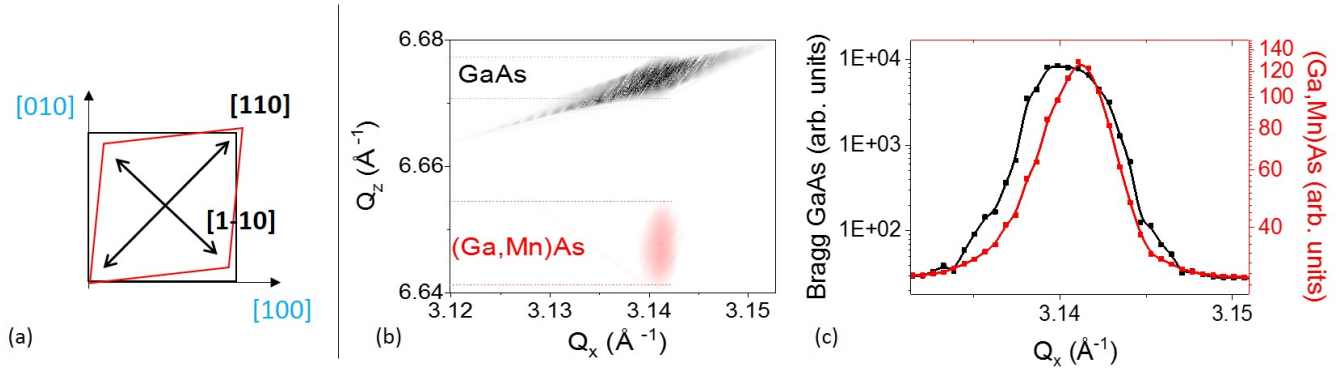

FIG. 3. (a) Schematics of a sheared in-plane (Ga,Mn)As lattice (in red) over GaAs (in black). In reciprocal space maps we look for misalignements of substrate and layer peak position along Q_x. (b) Reconstructed Q_x/Q_z map for the (226) diffraction peak (log scale). (c) Projection along the Q_x direction of substrate and layer diffraction peaks averaged between the dotted lines of (b), evidencing a slight shift, but which is of the same order of magnitude between consecutive and opposite peaks. Experiments are performed at room temperature.

searched inconclusively for signatures of anisotropic coherence length (i.e anisotropic (226) layer peak widths), and anisotropic structure factor (i.e anisotropic ratio of integrated intensity of GaAs and (Ga,Mn)As peaks).

Typical results obtained in the (C2) configuration are shown in Fig. 4(b,c). A clear and reproducible angular $\Delta\phi$=-2±0.3 mdeg was observed for the (226) direction. This (226) misalignment had the same sign for two consecutive azimuths, which should indicate a bulk rotation of the layer IP lattice with respect to the substrate, rather than a shearing. However, no misalignement was observed on (206) peaks (within the standard deviation) to validate this bulk rotation. As for the (C1) configuration, no robust evidence of a shear strain could be found in this high IP anisotropy layer.

Photoelastic effect

We turned to another method with a potentially larger sensitivity to strain: the photoelastic effect.

Owing to the photoelastic effect, the dielectric permittivity tensor of a zinc blende crystal is modified [60]. The biaxial strain does not induce any birefringence but an ϵ_{xy} shear strain introduces an off-diagonal matrix element that produces different refractive indices for linear polarization along the [110] and [-110] crystallographic axes. Consequently, for near-normal incidence, a linear polarization making an angle β with the [110] direction will rotate by an angle $\Delta\beta_{pe} = \Delta\beta^0_{pe}\sin(2\beta)$ with:

$$\Delta\beta^0_{pe} = Re\left[\frac{C_{44}P_{44}\epsilon_{xy}\left(1-\exp\left(i\frac{4\pi nt}{\lambda}\right)\right)}{n\left(n^2-1\right)}\right], \qquad (11)$$

where n is the complex refractive index (we assume the same index for the (Ga,Mn)As layer and the GaAs substrate), t the layer thickness, C_{44} the elastic constant, $P_{44} = 4P_{1212}$ with P the stress-optical tensor [61, 62]. It is this exact term that was used for the static or time-resolved detection of SAW-induced variations of strain in Refs. [27, 63]. Taking the experimental values for P_{44} and n from ref. [61] at the optical wavelength λ =532 nm and ϵ_{xy}=10^{-4} we estimate $\Delta\beta^0_{pe} \approx 15$ mdeg, which should be easily detected using a photoelastic modulator [64]. Once again, if it is a real shear strain that induces the IP anisotropy, it should persist at room temperature.

Four samples were investigated: Sample A with strong IP uniaxial anisotropy, sample B with biaxial anisotropy, an epiready GaAs substrate, and a 100 nm Aluminum layer evaporated on a glass substrate.

The polarization rotation was measured at room temperature in the reflection geometry as a function of the angle between an IP crystallographic axis (or an arbitrary axis in the case of Al/glass) and the incident linear polarization using a photoelastic modulator. In order to rotate the sample in its plane without any change in the path of the reflected light, the sample was mounted on an X-ray goniometer. The sample plane was perpendicular to the plane of incidence. The angle of incidence was 19°. The 532 nm-laser beam was linearly polarized perpendicular to the plane of incidence. The reflected beam was modulated by a photoelastic modulator (frequency f=42 kHz) with axes parallel and perpendicular to the incident polarization before passing through an analyser set at 45° to the axes and being detected by a photodiode. The Kerr rotation signal was detected at $2f$ by a lock-in amplifier. The reflected signal at the frequency of

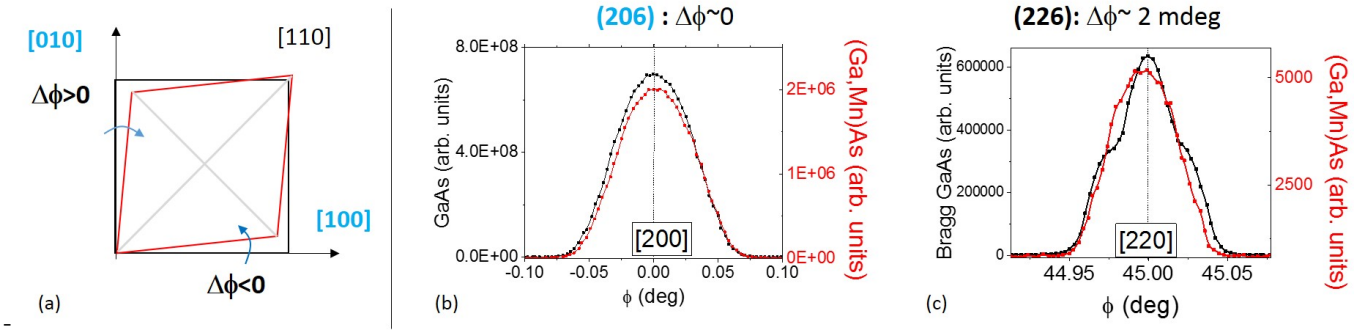

FIG. 4. (a) Schematics of sheared in-plane lattice. In (ϕ)-scans, we look for misalignments of <100> directions between the (Ga,Mn)As (in red) and GaAs (in black) lattice. (b) Typical ϕ-scans for (206) planes, with ω=15.8238° (resp. ω=15.6280°) for the Bragg (resp. (Ga,Mn)As) peak. (c) Typical ϕ-scans for (226) planes, with ω=10.9522° (resp. ω=10.8197°) for the GaAs (resp. (Ga,Mn)As) peak. We define $\Delta\phi$=$\phi_{GaAs} - \phi_{(Ga,Mn)As}$. "Wings" appear on either side of the GaAs substrate peak, a possible signature of truncation rods. Experiments are performed at room temperature.

a mechanical chopper was used to normalize the signal.

Figure 5 shows the polarization rotation for the four samples. For the Al/glass sample (triangles) there is hardly any dependence on the rotation angle, likewise for Sample B with biaxial anisotropy (full circles). Sample A, with uniaxial anisotropy (squares), shows a sin(2β) dependence, indeed related to the crystallographic axes as we have checked, but with an amplitude of less than 1.5 mdeg, i.e. ten times smaller than expected for ϵ_{xy}=10^{-4}. This places an upper boundary for a genuine shear strain in the layer of ϵ_{xy}=10^{-5}, just below our X-ray detection threshold. However, this polarization rotation is probably related to the GaAs, since it is the same on sample A and the bare substrate (empty circles). Since there is no such polarization rotation on sample B, this might depend on the quality of the substrate.

Therefore we conclude that the expected shear strain is not found although well within the detectability range of the optical measurements.

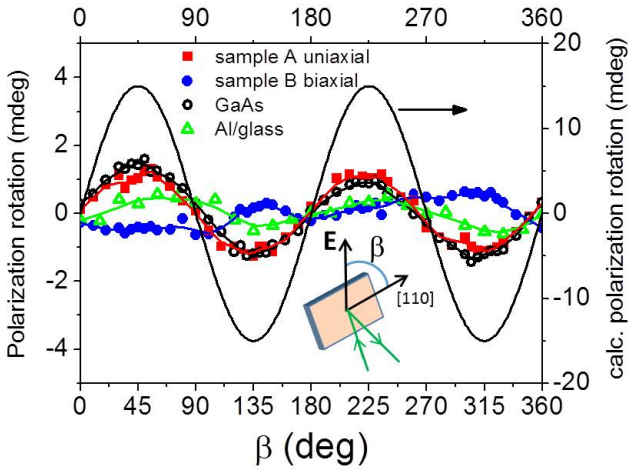

FIG. 5. Polarization rotation angle $\Delta\beta$ (left scale) as a function of β, the angle of rotation of the sample in its plane, for a fixed vertical light polarization **E**. For Sample A, Sample B and the GaAs substrate β is counted from the [110] axis as indicated in the inset. Right scale: the polarization rotation expected from the photoelastic effect assuming ϵ_{xy}=10^{-4}.

DISCUSSION AND CONCLUSION

We looked for experimental evidence of a structural shear strain being at the roots of strong in-plane magnetic anisotropy in (Ga,Mn)As, relying on X-ray diffraction or photoelastic effect-induced optical polarization rotation. While the search for anisotropic [110] and [1-10] vector lengths proved inconclusive due to poor experimental reproducibility, that of [100]/[010] angles differing from 90° clearly ruled out the existence of a physical ϵ_{xy}=10^{-4} strain compatible with the **k.p** theory estimations of our anisotropy. This was confirmed by photoelastic effect measurements. We thus conclude on the absence of a *physical* shear strain responsible for the observed uniaxial anisotropy, and instead on a mechanism capable of being modelled as an *effective* shear strain.

Paralleling the preferential attachment of Fe atoms to As-rich planes leading to strong uniaxial uniaxial anisotropy observed on Fe/GaAs [12] one can invoke the possible anisotropic incorporation of Mn atoms [25], or Mn dimer formation [13, 23] when growing (Ga,Mn)As on a GaAs substrate. These would be equivalent to a shear strain in a hypothetical free (Ga,Mn)As layer, thereby inducing magnetic anisotropy as the theory developed above shows, but be undetectable once epitaxied perfectly onto the substrate. Quite challenging to observe directly by microscopy techniques, such an anisotropic magnetic atom distribution might however show up as a measurable anisotropy of the exchange constant (at low temperature). A positive conclusion to such an experiment would help to devise growth strategies capable of tuning

this magnetic anisotropy. Independently of the origins of this effective shear strain, our comparison of data taken on a large number of articles highlights that the surest way of obtaining a strong IP anisotropy in (Ga,Mn)As remains to target a large *out-of-plane* anisotropy, often the result of a combination of large lattice mismatch, optimized anneal, and high effective Mn concentration.

ACKNOWLEDGMENTS

This work was financially supported by the Tunisian Ministry of Higher Education and Scientific Research, and by the French Ministry of Foreign Affairs through the project PHC Utique 16G1303. We acknowledge the SOLEIL Synchrotron for providing the beamtime for the diffraction experiments. We thank H. J. von Bardeleben from INSP for the FMR data and F. Vidal and M. Vabre from INSP for providing and fixing the X-ray goniometer for optical experiments.

* thevenard@insp.jussieu.fr

[1] S. Iwasaki, IEEE Transactions on Magnetics **16**, 71 (1980).
[2] L. Thevenard, B. Boutigny, N. Güsken, L. Becerra, C. Ulysse, S. Shihab, A. Lemaître, J.-V. Kim, V. Jeudy, and C. Gourdon, Physical Review B **95**, 054422 (2017).
[3] S. Davis, J. A. Borchers, B. B. Maranville, and S. Adenwalla, Journal of Applied Physics **117**, 063904 (2015).
[4] I. Camara, J.-Y. Duquesne, A. Lemaître, C. Gourdon, and L. Thevenard, Physical Review Applied **11**, 014045 (2019).
[5] D. Givord, O. F. K. McGrath, C. Meyer, and J. Rothman, Journal of Magnetism and Magnetic Materials **157-158**, 245 (1996).
[6] J. Zemen, J. Kučera, K. Olejník, and T. Jungwirth, Physical Review B **80**, 155203 (2009).
[7] J. Li and P. M. Haney, Applied Physics Letters **109**, 032405 (2016).
[8] O. Thomas, Q. Shen, P. Schieffer, N. Tournerie, and B. Lépine, Physical Review Letters **90**, 017205 (2003).
[9] S. Zhou, L. Chen, A. Shalimov, J. Zhao, and M. Helm, AIP Advances **2**, 042102 (2012).
[10] E. M. Kneedler, B. T. Jonker, P. M. Thibado, R. J. Wagner, B. V. Shanabrook, and L. J. Whitman, Physical Review B **56**, 8163 (1997).
[11] M. Zölfl, M. Brockmann, M. Köhler, S. Kreuzer, T. Schweinböck, S. Miethaner, F. Bensch, and G. Bayreuther, Journal of Magnetism and Magnetic Materials **175**, 16 (1997).
[12] K. Tivakornsasithorn, X. Liu, X. Li, M. Dobrowolska, and J. K. Furdyna, Journal of Applied Physics **116**, 043915 (2014).
[13] M. Birowska, C. Śliwa, J. A. Majewski, and T. Dietl, Physical Review Letters **108**, 237203 (2012).
[14] Y. Hashimoto, Y. Iye, and S. Katsumoto, Journal of Crystal Growth **378**, 381 (2013).
[15] U. Welp, V. K. Vlasko-Vlasov, A. Menzel, H. D. You, X. Liu, J. K. Furdyna, and T. Wojtowicz, Applied Physics Letters **85**, 260 (2004).
[16] J. Wunderlich, A. C. Irvine, J. Zemen, V. Holý, A. W. Rushforth, E. De Ranieri, U. Rana, K. Výborný, J. Sinova, C. T. Foxon, R. P. Campion, D. A. Williams, B. L. Gallagher, and T. Jungwirth, Physical Review B **76**, 054424 (2007).
[17] J. Shiogai, D. Schuh, W. Wegscheider, M. Kohda, J. Nitta, and D. Weiss, Applied Physics Letters **98**, 98 (2011).
[18] M. Sawicki, K.-Y. Wang, K. W. Edmonds, R. P. Campion, C. R. Staddon, N. R. S. Farley, C. T. Foxon, E. Papis, E. Kamińska, A. Piotrowska, T. Dietl, and B. L. Gallagher, Physical Review B **71**, 121302 (2005).
[19] S. Piano, X. Marti, a. W. Rushforth, K. W. Edmonds, R. P. Campion, M. Wang, O. Caha, T. U. Schülli, V. Holý, and B. L. Gallagher, Applied Physics Letters **98**, 152503 (2011).
[20] S. van Dijken, G. Di Santo, and B. Poelsema, Applied Physics Letters **77**, 2030 (2000).
[21] A. Muñoz-Noval, E. Salas-Colera, and R. Ranchal, The Journal of Physical Chemistry C **123**, 13131 (2019).
[22] A. W. Rushforth, E. De Ranieri, J. Zemen, J. Wunderlich, K. W. Edmonds, C. S. King, E. Ahmad, R. P. Campion, C. T. Foxon, B. L. Gallagher, K. Výborný, J. Kučera, and T. Jungwirth, Physical Review B **78**, 085314 (2008).
[23] M. Birowska, Journal of Magnetism and Magnetic Materials **432**, 396 (2017).
[24] H. Subramanian and J. E. Han, Journal of Physics: Condensed Matter **25**, 206005 (2013).
[25] M. Kopecký, J. Kub, F. Máca, J. Mažek, O. Pacherová, A. W. Rushforth, B. L. Gallagher, R. P. Campion, V. Novák, and T. Jungwirth, Physical Review B **83**, 235324 (2011).
[26] P. Kuszewski, I. S. Camara, N. Biarrotte, L. Becerra, J. von Bardeleben, W. Savero Torres, A. Lemaître, C. Gourdon, J.-Y. Duquesne, and L. Thevenard, Journal of Physics: Condensed Matter **30**, 244003 (2018).
[27] P. Kuszewski, J.-Y. Duquesne, L. Becerra, A. Lemaître, S. Vincent, S. Majrab, F. Margaillan, C. Gourdon, and L. Thevenard, Physical Review Applied **10**, 034036 (2018).
[28] D. K. Biegelsen, R. D. Bringans, J. E. Northrup, and L.-E. Swartz, Physical Review B **41**, 5701 (1990).
[29] Q. Xue, T. Hashizume, J. M. Zhou, T. Sakata, T. Ohno, and T. Sakurai, Physical Review Letters **74**, 3177 (1995).
[30] M. S. Brandt, S. T. B. Goennenwein, T. A. Wassner, F. Kohl, A. Lehner, H. Huebl, T. Graf, M. Stutzmann, A. Koeder, W. Schoch, and A. Waag, Applied Physics Letters **84**, 2277 (2004).
[31] S. T. B. Goennenwein, T. Graf, T. Wassner, M. S. Brandt, M. Stutzmann, J. B. Philipp, R. Gross, M. Krieger, K. Zurn, P. Ziemann, A. Koeder, S. Frank, W. Schoch, and A. Waag, Applied Physics Letters **82**, 730 (2003).
[32] P. Němec, V. Novák, N. Tesařová, E. Rozkotová, H. Reichlová, D. Butkovičová, F. Trojánek, K. Olejník, P. Malý, R. Campion, B. Gallagher, J. Sinova, and T. Jungwirth, Nature Communications **4**, 1422 (2013).
[33] A. Chernyshov, M. Overby, X. Liu, J. K. Furdyna, Y. Lyanda-Geller, and L. P. Rokhinson, Nature Physics **5**, 656 (2009).

[34] D. Fang, H. Kurebayashi, J. Wunderlich, K. Výborný, L. P. Zârbo, R. P. Campion, A. Casiraghi, B. L. Gallagher, T. Jungwirth, and A. J. Ferguson, Nature Nanotechnology **6**, 413 (2011).

[35] V. K. Vlasko-Vlasov, W. K. Kwok, S. Dong, X. Liu, M. Dobrowolska, and J. K. Furdyna, Physical Review B **98**, 1 (2018).

[36] K. Khazen, H. von Bardeleben, J. Cantin, L. Thevenard, L. Largeau, O. Mauguin, and A. Lemaître, Physical Review B **77**, 165204 (2008).

[37] Using Fig. 4 of Ref. 32, we calculated their $K_{2\parallel}$ and $K_{2\perp}$ using $K_{out}(mT)$=$B_{2\perp}$-$\mu_0 M_s/2$ and assumed that all Mn were magnetically active to convert their anisotropy fields (K_{out}, K_u) into anisotropy constants.

[38] S. Haghgoo, M. Cubukcu, H. J. von Bardeleben, L. Thevenard, A. Lemaître, and C. Gourdon, Physical Review B **82**, 041301(R) (2010).

[39] L. Thevenard, C. Gourdon, S. Haghgoo, J.-P. Adam, H. J. von Bardeleben, A. Lemaître, W. Schoch, and A. Thiaville, Physical Review B **83**, 245211 (2011).

[40] L. Thevenard, E. Peronne, C. Gourdon, C. Testelin, M. Cubukcu, E. Charron, S. Vincent, A. Lemaître, and B. Perrin, Physical Review B **82**, 104422 (2010).

[41] M. Cubukcu, H. J. von Bardeleben, K. Khazen, J. L. Cantin, O. Mauguin, L. Largeau, and A. Lemaître, Physical Review B **81**, 041202 (2010).

[42] H. Riahi, W. Ouerghui, L. Thevenard, C. Gourdon, M. Maaref, A. Lemaître, O. Mauguin, and C. Testelin, Journal of Magnetism and Magnetic Materials **342**, 149 (2013).

[43] S. Shihab, H. Riahi, L. Thevenard, H. J. von Bardeleben, A. Lemaître, and C. Gourdon, Applied Physics Letters **106**, 142408 (2015).

[44] F. Matsukura and H. Ohno, Japanese Journal of Applied Physics **54**, 098003 (2015).

[45] J. M. Luttinger and W. Kohn, Physical Review **97**, 869 (1955).

[46] M. Yahyaoui, K. Boujdaria, M. Cubukcu, C. Testelin, and C. Gourdon, Journal of Physics: Condensed Matter **25**, 346001 (2013).

[47] O. Madelung, U. Rossler, and M. Schulz, Landolt-Bornstein, New Series, Group III, Springer-Vela, Berlin **41** (2005).

[48] T. Dietl, H. Ohno, F. Matsukura, J. Cibert, and e. D. Ferrand, science **287**, 1019 (2000).

[49] T. Dietl, H. Ohno, and F. Matsukura, Physical Review B **63**, 195205 (2001).

[50] G. Pikus and G. Bir, Tverd. Tela (Leningrad) **1**, 1642 (1960).

[51] G. G. Koster, J. Dimmock, R. G. Wheeler, and H. Statz, *Properties of the thirty-two point groups*, Vol. 24 (The MIT Press, 1963).

[52] The basis wave functions used for the matrix representation of $\mathcal{H}_S$ are extracted from the table 83, p. 94, of Koster *et al* [51] representing the direct product of two irreducible representations, namely $\Gamma_5 \otimes \Gamma_6 = \Gamma_7 + \Gamma_8$. In this table, ($u^5_{yz}$, u^5_{xz}, u^5_{xy}) indicate (X, Y, Z) p orbitals, $v^6_{1/2}$=$\uparrow$ and $v^6_{-1/2}$=$\downarrow$ where $\uparrow$ ($\downarrow$) indicates spin up (spin down) states. $\psi^7_{-1/2} = |\frac{1}{2}, -\frac{1}{2}>$ and $\psi^7_{1/2} = |\frac{1}{2}, \frac{1}{2}>$ represent the usual split-off valence bands (VBs), $\psi^8_{-3/2} = |\frac{3}{2}, \frac{1}{2}>$ and $\psi^8_{3/2} = |\frac{3}{2}, -\frac{1}{2}>$ indicate the light-hole VBs, $\psi^8_{-1/2} = |\frac{3}{2}, \frac{3}{2}>$ and $\psi^8_{1/2} = |\frac{3}{2}, -\frac{3}{2}>$ represent the heavy-hole VBs.

[53] M. Glunk, J. Daeubler, L. Dreher, S. Schwaiger, W. Schoch, R. Sauer, W. Limmer, A. Brandlmaier, S. Goennenwein, C. Bihler, *et al.*, Physical Review B **79**, 195206 (2009).

[54] I. Vurgaftman, J. Á. Meyer, and L. á. Ram-Mohan, Journal of applied physics **89**, 5815 (2001).

[55] M. Yahyaoui, C. Testelin, C. Gourdon, and K. Boujdaria, Journal of Applied Physics **111**, 033902 (2012).

[56] E. du Trémolet de Lacheisserie, D. Gignoux, and M. Schlenker, eds., *Magnetism I- Fundamentals* (Kluwer Academic Publishers, 2003).

[57] R. Grössinger, R. S. Turtelli, and N. Mehmood, in *IOP Conference Series: Materials Science and Engineering*, Vol. 60 (IOP Publishing, 2014) p. 012002.

[58] S. C. Masmanidis, H. X. Tang, E. B. Myers, M. Li, K. De Greve, G. Vermeulen, W. Van Roy, and M. L. Roukes, Physical Review Letters **95**, 187206 (2005).

[59] T. U. Schülli, M. Sztucki, V. Chamard, T. H. Metzger, and D. Schuh, Applied Physics Letters **81**, 448 (2002).

[60] D. Royer and E. Dieulesaint, *Elastic Waves in Solids* (Springer-Verlag, Heidelberg, 2001).

[61] P. Etchegoin, J. Kircher, M. Cardona, C. Grein, and E. Bustarret, Physical Review B **46**, 15139 (1992).

[62] M. Cardona, D. Rönnow, and P. V. Santos, Thin Solid Films **313**, 10 (1998).

[63] P. V. Santos, Applied Physics Letters **74**, 4002 (1999).

[64] K. Sato, Japanese Journal of Applied Physics **20**, 2403 (1981).